Macromolecules

pubs.acs.org/Macromolecules
Article

Entropic Penalty Switches Li^+ Solvation Site Formation and Transport Mechanisms in Mixed Polarity Copolymer Electrolytes

Chuting Deng, Peter Bennington, Regina J. Sánchez-Leija, Shrayesh N. Patel, Paul F. Nealey, and Juan J. de Pablo*

Cite This: *Macromolecules* 2023, 56, 8069–8079
Read Online

ABSTRACT: Emerging solid polymer electrolyte (SPE) designs for efficient Li-ion (Li^+) conduction have relied on polarity and mobility contrast to improve conductivity. To further develop this concept, we employ simulations to examine Li^+ solvation and transport in poly(oligo ethylene methacrylate) (POEM) and its copolymers with poly(glycerol carbonate methacrylate) (PGCMA). We find that Li^+ is solvated by ether oxygens instead of the highly polar PGCMA, due to lower entropic penalties. The presence of PGCMA promotes single-chain solvation, thereby suppressing interchain Li^+ hopping. The conductivity difference between random copolymer PGCMA-*r*-POEM and block copolymer PGCMA-*b*-POEM is explained in terms of a hybrid solvation site mechanism. With diffuse microscopic interfaces between domains, PGCMA near the POEM contributes to Li^+ transport by forming hybrid solvation sites. The formation of such sites is hindered when PGCMA is locally concentrated. These findings help explain how thermodynamic driving forces govern Li^+ solvation and transport in mixed SPEs.

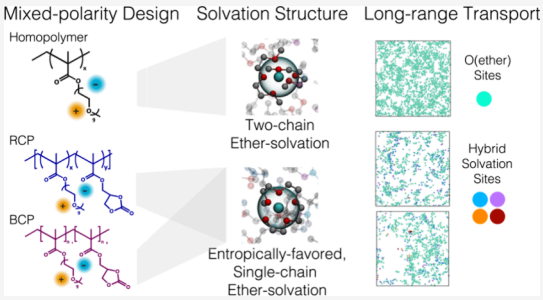

INTRODUCTION

Solid polymer electrolytes (SPE) in Li-ion (Li^+) batteries must exhibit high conductivity, mechanical strength, and high transference number to achieve good cycling performance and fast charging rates and to prevent Li dendrite growth.[1,2] Poly(ethylene oxide) (PEO) is perhaps the most widely studied polymer host for Li^+ transport to date, and past work has shown that it does not meet these three criteria.[3,4] In attempts to overcome its inherent limitations, PEO is often mixed with other materials to improve the conductivity or to incorporate additional functionalities. Previous efforts have sought to blend PEO with plasticizers,[5] copolymerize it with high-T_g polymers such as poly(styrene) (PS) to form a phase-separated block copolymer (BCP),[6−10] and copolymerize it with single-ion conductors.[11] These three strategies have been found to increase the ionic conductivity, improve the mechanical strength, and increase the transference number, respectively.

Studies of mixed liquid electrolytes have shown that polarity and mobility contrast can be combined to improve conductivity relative to that of the pure components.[12] These small-molecule systems typically blend a high-polarity solvent, such as ethylene carbonate (EC), with a low-viscosity solvent, such as dimethyl carbonate (DMC). The high dielectric constant of the former facilitates salt dissociation, whereas the low viscosity of the latter provides a high-mobility medium for Li^+-EC complexes to diffuse. However, achieving this synergistic coupling can be challenging in polymeric systems. This is because ion solvation and transport in mixed SPEs cannot be anticipated solely based on the individual properties of each component. Instead, it emerges from the interplay of multiple factors, such as polarity,[13] chemical structure,[14,15] miscibility,[16−19] solvation site connectivity,[20−22] and segmental dynamics,[20,22,23] to name a few. On the one hand, in SPE, specific chemical structures can favorably solvate Li^+ despite a relatively low polarity. Particularly, Li^+ solvation by poly- or oligoether motifs is found to be important in the presence of other functional groups having higher polarity. Studies have shown that in poly(oligo ethylene methacrylate) (POEM), Li^+ is primarily solvated by the ether side chains, even if the carbonyl oxygen on the backbone is more polar.[20,22] Similarly, when EC is mixed with an oligoether, the less polar oligoether chains are primarily responsible for solvating Li^+.[24] On the other hand, Li^+ transport occurs through different mechanisms in liquid electrolytes and in SPEs. In a mixed liquid electrolyte, the enhanced Li^+ transport is achieved via the vehicular diffusion of Li^+-solvent complexes through a low-viscosity medium.[12] In contrast, in high-molecular-weight SPEs, such vehicular diffusion is inhibited[4] and Li^+ transport

Received: April 25, 2023
Revised: August 23, 2023
Published: September 22, 2023

https://doi.org/10.1021/acs.macromol.3c00804
Macromolecules 2023, 56, 8069−8079

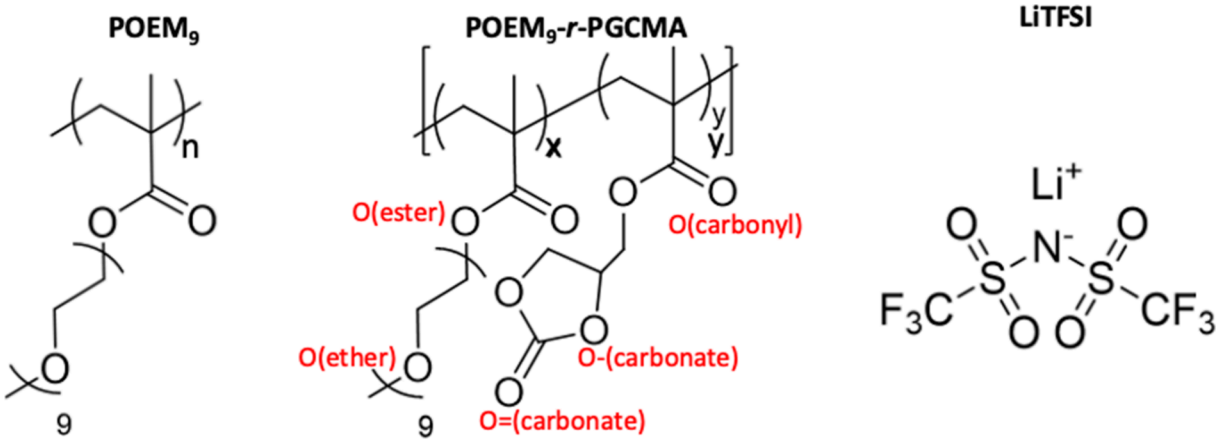

Figure 1. Chemical structures of POEM, POEM-*r*-PGCMA, and LiTFSI salt. Salt concentration is determined as $r = [Li^+]/([EO] + [OCOO]) = 0.05$. Different oxygen types are labeled in red.

occurs through discrete hopping events from one solvation site to another.[14,25] This mechanism in turn relies on both fast segmental dynamics and the connectivity of solvation sites,[20−22] which can be altered dramatically when polymers are mixed with other components. Studies of Li^+ transport in mixed polymeric materials have been limited, and a mechanistic understanding of the underlying molecular processes is still lacking. Past reports of mixed SPE materials have typically involved a high-T_g, nonconducting polymer mixed with a rubbery ion-conducting polymer to improve the mechanical strength.[16−18,26,27] In those systems, the nonconducting components are found to not only slow down the segmental dynamics of the conducting component[18,28,29] but also disrupt the conducting network.[16,17,26,29] As the degree of miscibility increases, interconnected solvation sites tend to disintegrate into clusters. As a result, long-range Li^+ in those blends is often found to involve two time scales, one associated with local Li^+ hopping within a cluster and another associated with transport between clusters upon network rearrangements.[26]

Since the mechanism for Li^+ transport in polymers differs from that in liquid electrolytes, one must consider the specific chemical characteristics of an SPE when designing polarity-mobility contrast. In this work, we build on the hypothesis that a suitable contrast of mobility and polarity in SPE systems is best achieved when the low-T_g, conductive PEO-based polymer is selected as the DMC analogue and a polymer containing highly polar cyclic carbonate groups is selected as the EC analog. In recent experiments from our group, the POEM/poly(glycerol carbonate methacrylate) (PGCMA) pair was shown to provide a desirable contrast of polarity and mobility.[29] Perhaps counterintuitively, experiments indicate that in LiTFSI-doped PGCMA-*r*-POEM, the highly polar cyclic carbonate interacts with the Li ions only minimally and the polyether segments are responsible for Li^+ solvation. Because the presence of PGCMA suppresses chain mobility without improving ion dissociation, the overall conductivity of PGCMA-r-POEM is lower than that of the POEM homopolymer electrolyte.

To gain a better understanding of Li^+ solvation and transport in PGCMA-*r*-POEM, we resort to atomistic molecular dynamics (MD) simulations and compare POEM and PGCMA-*r*-POEM (Figure 1), each blended with a LiTFSI salt at $r = 0.05$. We find that the slowdown of the overall chain dynamics due to PGCMA can be corrected via a simple renormalization by T_g of the mixture. A subsequent analysis of the underlying structures reveals that Li^+ solvation by highly polar PGCMA is rare and transient. In contrast, Li^+-ether solvation is entropically favored. This suggests that entropic penalties, which can be pronounced in SPEs, lead to fundamentally different solvation tendencies compared to those encountered in liquid electrolytes. Our findings also show that the diluting effects of PGCMA suppress interchain hopping by promoting single-chain solvation, thereby decreasing the efficiency of solvating oxygens for Li^+ transport. This concept is developed by studying PGCMA-*b*-POEM, where one can observe the formation of local compositional fluctuations or small domains. In PGCMA-*b*-POEM, the formation of solvating sites is further decreased with respect to that in the random copolymer; transient PGCMA-rich regions are inactive for transport and interrupt the connectivity of solvation sites in favor of isolated clusters. More generally, the results presented in this work provide a direct characterization of how local heterogeneities and mixing influence local and long-range Li^+ transport in mixed SPEs, thereby providing useful principles for the design of new SPE systems.

METHODS

United Atom Model and Partial Charge Assignments. The polymers considered here are represented by united atoms. For POEM units, all interaction parameters are taken from an adapted Trappe-UA force field,[30−32] previously validated to match the experimental properties, including density, of PEO.[33] Li^+ and $TFSI^-$ are represented by a compatible all-atom model.[34,35] For the cyclic carbonate units, the bonded parameters and the short-range Lennard−Jones (LJ) parameters are adopted from the Trappe-UA force field[31,32,36,37] and a cyclic carbonate force field.[38] The LJ parameters of the cyclic carbonate are scaled to match the Li^+−O═(carbonate) radial distribution function[39] and densities of liquid EC and PC measured in experiments.[38] Partial charges for polymer interaction sites are refined through *DFT* calculations using a B3LYP functional and the 6-31G(d,p) basis set, performed with the GAUSSIAN 09 program.[40] The charge fitting uses the ChElPG calculation scheme.[41] A charge scaling of 0.7 is applied to Li^+ and $TFSI^-$ as a mean-field treatment for polarization effects.[42] Detailed force field parameters, a protocol for partial charge assignment, and procedures for initial configuration generation are provided in the Supporting Information.

MD Simulation Parameters. The simulations are performed using the LAMMPS package.[43] For LJ interactions, a cutoff radius of

https://doi.org/10.1021/acs.macromol.3c00804
Macromolecules 2023, 56, 8069−8079

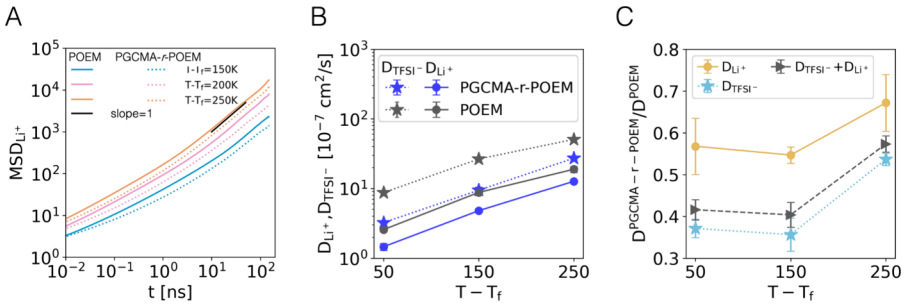

Figure 2. (A) Mean squared displacements (MSD) of Li^+ in POEM and PGCMA-*r*-POEM at 150, 200, and 250 K above their fictive temperature, T_f. (B) Diffusion coefficients of Li (D_{Li}) and TFSI (D_{TFSI}) in the POEM and PGCMA-*r*-POEM. MSD between 20 and 120 ns are used to determine the diffusion coefficients using the Einstein relation. The error bars are estimated based on the difference in the diffusion coefficient obtained from fits over the first and second halves of the fit interval. (C) Ratio of diffusion coefficients in POEM and PGCMA-*r*-POEM. Error bars in (C) are based on propagation from (B).

12 Å with a van der Waals tail correction is used. The long-range Coulombic interactions use a cutoff radius of 12 Å and are handled using the particle−particle particle−mesh solver with 10^{-4} accuracy.[44] The trajectories are integrated using the velocity-Verlet algorithm with a 1 fs time step. For NVT simulations, the Nosé−Hoover thermostat with a damping parameter of 100 fs is used. For NPT simulations, the Nosé−Hoover barostat with a damping parameter of 1000 fs is applied in addition to the thermostat. Additional details about the simulation procedures are included in the Supporting Information.

RESULTS AND DISCUSSION

In this section, we present simulation results that compare ion solvation tendencies and transport in LiTFSI-doped PGCMA-*r*-POEM (50 wt %) to that in the POEM homopolymer electrolyte. Figure 1 shows the chemical structures and introduces the nomenclature for the different oxygen types used in this study. Here the salt concentration is $r = [Li^+]/([EO] + [OCOO]) = 0.05$, under the assumption that both O(ether) and O═(carbonyl) are expected to be potential Li^+-solvating units. The rest of the Results and Discussion section is organized as follows: in the first two parts, we compare the ion-segmental dynamics and ion solvation, respectively, before and after the incorporation of PGCMA. The third part examines the implication of the altered ion solvation tendency, due to the presence of PGCMA, on Li^+ transport mechanisms locally and over the long range.

Ion Mobilities Were Reduced by Half after Renormalizing by T_g. In SPEs, Li^+ conductivity is intrinsically coupled to the segmental dynamics of the polymer matrix, typically described via the Vogel−Fulcher−Tammann (VFT) equation.[18,45] This is due to the intersegmental hopping of Li^+, which is the major transport mechanism in SPEs and relies on conformational rearrangements of ion-solvating segments.[25] We first compute the fictive glass transition temperature (T_f) of PGCMA-*r*-POEM and POEM (Table S1). Experimentally, the addition of 40 wt % PGCMA was reported to raise the T_g by ca. 50 K.[29] Consistent with experiments, the simulated T_f is increased by 37 K after 50 wt % PGCMA is incorporated into the mixed system. To isolate any intrinsic effects of side-chain architecture and copolymer polarity, our production simulation runs are performed at a fixed temperature relative to T_f of the mixture to account for differences in the average segmental mobility of the materials.

Figure 2 summarizes the simulated diffusion coefficients of ions in the POEM and PGCMA-*r*-POEM at fixed temperatures above T_f. The two materials show significant differences in ion diffusion after normalization with respect to T_f, suggesting that additional mechanisms beyond segmental dynamics and the VFT equation are involved. Figure 2A presents the mean squared displacements (MSD) of Li^+ for different time intervals. For time intervals below 1 ns, Li^+ motion is subdiffusive, as indicated by a slope of less than unity on a log−log scale. At time scales greater than 10 ns, Li^+ motion is diffusive, as indicated by a unit slope. The self-diffusion coefficients of Li^+ (D_{Li}) and $TFSI^-$ (D_{TFSI}), obtained by performing a linear fit to the MSD, are reported in Figure 2B as a function of the reduced temperature. At 50−250 K above T_f, the diffusion coefficient of Li^+ ranges between 1 and 10×10^{-7} cm^2/s. At $r = 0.05$, which corresponds to a relatively dilute salt concentration, the correlated motion between cations and anions is found to be negligible (Figure S5); the sum of D_{Li} and D_{TFSI} is therefore directly proportional to the equivalent conductivity via the Nernst−Einstein equation.[25] Figure 2C reports the ratios of the diffusion coefficients in PGCMA-*r*-POEM to those in POEM. At 50 and 150 K above T_f, the Li^+ diffusivity in PGCMA-*r*-POEM is reduced by 45%, and the $TFSI^-$ diffusivity is reduced by roughly 64%, leading to a drop in conductivity of approximately 60%. The simulated results for ionic diffusivity are consistent with the experimental conductivity measurements reported by Bennington et al.,[29] where a two-fold decrease was observed in PGCMA-*r*-POEM with a similar composition (58 wt % of POEM) at a similar reduced temperature above T_g. As the temperature increases to 250 K above T_f, the reduction in ion diffusivities becomes less prominent.

The following analysis examines how the transport of Li^+ occurs in PGCMA-*r*-POEM by dissecting the local segmental motions and the solvation environment of Li^+.

Mobilities of Ion and Ion-Solvating Segments at Fixed Temperature Above T_g. Renormalizing the temperature by T_g is generally effective for explaining the effect of the segmental dynamics on the ionic conductivity. For systems with side-chain architectures such as POEM, however, our recent work suggests that this is not the case. In POEM, the segmental dynamics vary along the ether side chain, which incorporates the ion-solvating segments that are most critical for Li^+ transport.[20,22] Because T_f and T_g reflect the average dynamics of the entire system, they fail to provide complete information about individual relaxation modes along the ether side chain. Apart from the side chain architecture, the mixing of glassy and mobile components is also thought to affect local segmental mobility.[26−28] In the PGCMA-*r*-POEM copolymer,

https://doi.org/10.1021/acs.macromol.3c00804
Macromolecules 2023, 56, 8069−8079

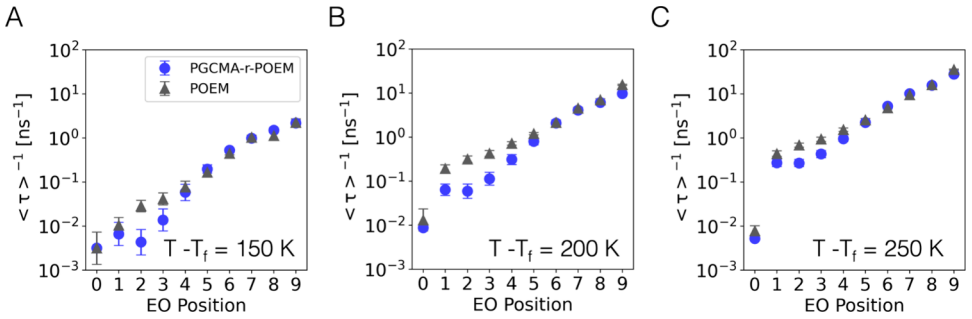

Figure 3. Inverse mean relaxation time extracted from BVAF for different ether oxygens along an OEM side chain in POEM and PGCMA-*r*-POEM at (A) $T - T_f = 150$ K, (B) $T - T_f = 200$ K, and (C) $T - T_f = 250$ K. An EO position of 1 refers to the ether oxygen that is closest to the backbone. The EO position of 0 refers to the backbone.

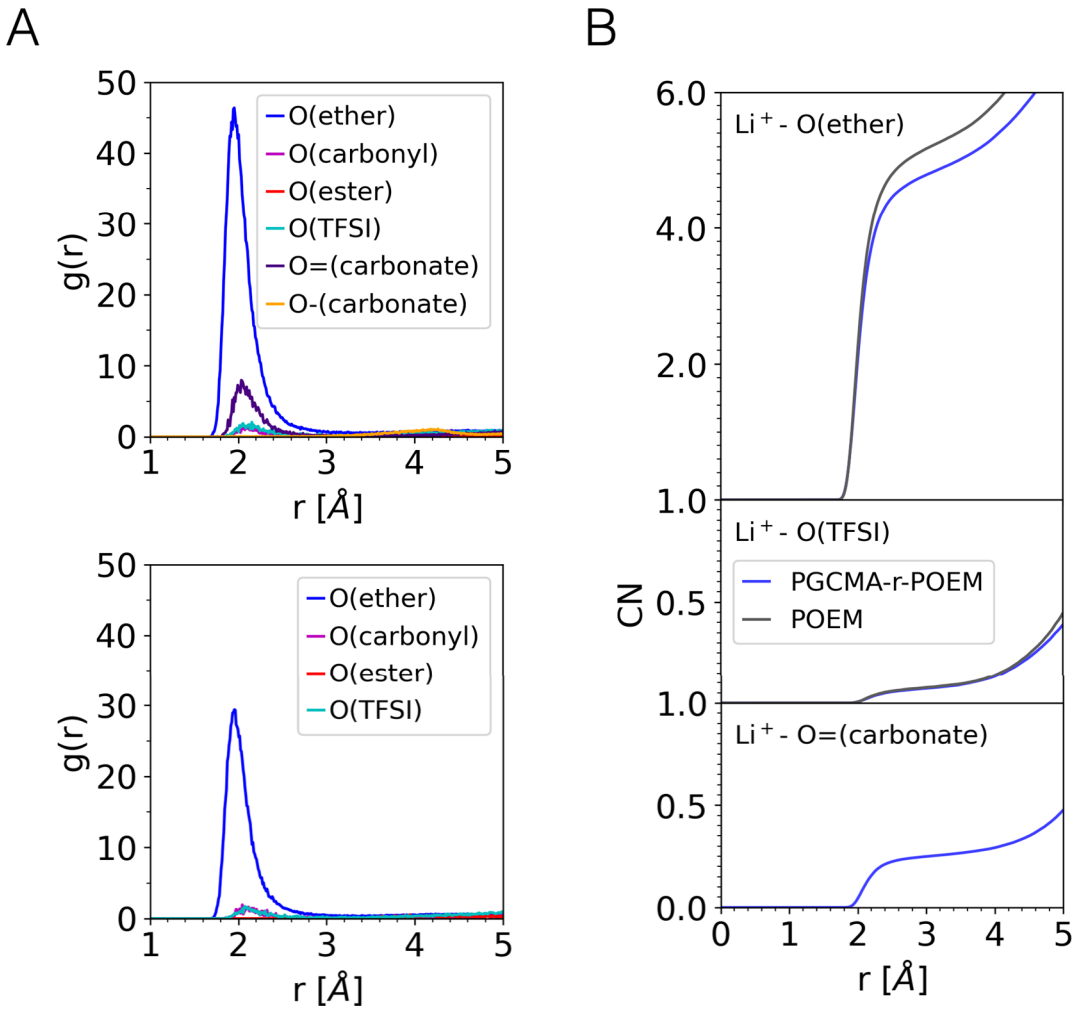

Figure 4. (A) Radial distribution functions between Li^+ and oxygen atoms in the PGCMA-*r*-POEM (top) and POEM (bottom). (B) Coordination numbers $CN_{ij}(r)$ in POEM and PGCMA-*r*-POEM between Li^+ and O(ether) (top), O(TFSI) (center), and O=(carbonate) (bottom).The results are obtained at 150 K above T_f.

PGCMA units could conceivably slow the segmental motions in their immediate vicinity. To examine the rate of each relaxation mode along the side chains, we compute the bond vector autocorrelation function (BVAF) for each C−O(ether) bond along the side chain.[20,22] This function quantifies how fast a vector connecting two bonded atoms becomes decorrelated from its initial orientation. Each BVAF is fitted to a stretched exponential function of the form $BVAF(t) = e^{-(t/\tau)^{\beta}}$, whose first moment is given by $<\tau> = (\beta/\tau)\Gamma(\beta - 1)$. The inverse mean relaxation time, $1/<\tau>$, is used to describe the local segmental mobility. Figure 3 compares the local segmental mobility along the side chain at three reduced temperatures. It increases with temperature as a result of faster side chains (positions 1−9), rather than more mobile backbones (position 0). At each temperature, ethers 1−3 in the random copolymer exhibit slower segmental mobility, possibly due to the presence of the PGCMA side chain, whereas ethers 4−7, the ion-solvating segments along the

https://doi.org/10.1021/acs.macromol.3c00804
Macromolecules 2023, 56, 8069−8079

POEM side chain (Figure S6 and ref 22), exhibit similar mobilities to those observed in POEM. Overall, despite the presence of the PGCMA pendant group, the segmental mobility of the backbone and that of the ion-solvating group are identical in POEM and the PGCMA-*r*-POEM. Segmental dynamics can be thought to affect ion transport at two length scales.[26] At the length scale of an immediate solvation shell (below 5 Å), Li^+ hopping between solvation sites is assisted by fluctuations in the local solvation structure. Beyond that scale, the long-range transport of Li^+ requires consecutive hopping events capable of traversing the solvation site network. Such a process is expected to benefit from a fast reorganization of the entire network of solvation sites.[21] The unaffected backbone relaxation after the addition of PGCMA suggests that the rate of solvation site network reorganization in the two systems is also comparable once the temperature is renormalized by T_g. To understand the origin of a factor of 2 difference in ion diffusivity between the two materials, whose local segmental mobilities are similar, we contrast their Li^+ solvation environments, including both the immediate solvation structure and the network of viable solvation sites.

Despite the High Polarity of the Cyclic Carbonate Group, It Is Entropically Favorable for Li^+ Ions To Be Primarily Solvated by Ether Segments. In mixed systems with synergistic solvent polarity and mobility, the high polarity facilitates salt dissociation, and the slower mobility is minimally coupled to ion diffusion or is offset by increases in the concentration of free carriers.[13,45,46] From simulations, the dipole moment of the cyclic carbonate group is estimated to be 5.14 D, and that of the C−O−C ethylene oxide group is around 1.83 D (Figure S3). The added cyclic carbonate groups increase the dielectric constant from 4.83 for the POEM homopolymer to 7.85 for PGCMA-*r*-POEM. Equations used for the dielectric constant are included in the SI. As has been shown in various studies, increased dielectric constant tends to reduce the correlated motion of oppositely charged ions.[47,48] Experimental studies of PGCMA-*r*-POEM, however, reveal that despite a high polarity, the cyclic carbonate group does not improve salt dissociation, and does not interact with Li^+ to any significant extent.[29] To gain insight into Li^+ solvation in these materials, we begin our analysis by computing the radial distribution function between Li^+ and different oxygen types, which we identify as potential coordinating sites. Figure 4A compares the sizes and compositions of the first solvation shells of Li^+ in POEM and PGCMA-*r*-POEM. In both systems, the first solvation peaks occur at around 2.0 Å, and the size of the first solvation shell, delineated by the first minimum, is determined to be ca. 3.25 Å. The first solvation shell consists of O(ether), O(TFSI), and O═(carbonate), each contributing differently, as indicated by their different peak heights. Additionally, we note that although the carbonyl oxygens in both the methacrylate group and the carbonate group are more polar than the O(ether), these carbonyl oxygens are absent in the first solvation shell.

To compare the first solvation shell compositions in POEM and PGCMA-*r*-POEM, we present their coordination numbers for each type of oxygen in Figure 4B. In both materials, the O(ether) predominately solvates Li^+ with a coordination number of around 5. However, compared to those in POEM, the Li^+−O(ether) and Li^+−O(TFSI) coordination in PGCMA-*r*-POEM both decrease by a small percentage and are replaced by Li^+−O═(carbonate) coordination. The added cyclic carbonate groups, which were expected to facilitate salt dissociation, decrease the interaction between Li^+ and $TFSI^-$ only slightly. The degree of salt dissociation depends strongly on Li^+−O(ether) interactions. In our simulations, the O═(carbonate) carries −0.5105 e, the O(ether) carries −0.4757 e, and the O(TFSI) carries −0.371 e, where e is the elementary charge. The relative contributions from O═(carbonate) and O(TFSI) are closely related to their negative partial charges in our model. Such an argument, however, is not sufficient to explain why O(ether) is the major Li^+-solvating oxygen despite its relatively low polarity. Our simulations, performed for two alternative sets of partial charge assignments, lead to similar observations and are discussed in the Supporting Information.

Despite the general expectation that ion dissociation is favored by high-polarity solvents, some specific chemistries have been reported to enhance solvation, even in the presence of other highly polar groups. For example, a study on polyether-polycarbonate copolymers reported that solvation by ether groups, particularly side-chain ethers, was favored over more polar carbonate groups.[14] Similar findings were observed in studies on POEM, which showed that Li^+ was exclusively solvated by ether groups, not by the more polar carbonyl oxygens of the methacrylate backbone.[20,22] Salt dissociation processes can be viewed as a competition among three thermodynamic driving forces: an unfavorable increase in enthalpy (lattice energy) from breaking up the underlying "lattice", a favorable decrease in enthalpy due to the interaction between ions and the solvent, and a favorable increase in entropy due to mixing. While high solvent polarity produces enthalpic gains, an additional entropy penalty arises in ion-polymer solvation due to several mechanisms. First, we note that entropy gains from mixing are usually small in generic polymer systems.[49] Second, there is an entropic penalty for a high concentration of dissociated ions, because they restrict the polymer conformation space by acting as cross-linking sites and by forming solvation structures with polymer segments that require specific chain conformations.[50,51]

These thermodynamic driving forces for Li^+ solvation explain the respective solvation tendencies of the POEM and PGCMA units in the studied materials. For PGCMA units to solvate a Li^+, approximately four cyclic carbonate side chains[39] must orient themselves toward the Li^+. Additionally, each solvation results in four anchored carbonate side chains, leading to additional conformational restrictions. In contrast, a single POEM side chain can readily supply nine contiguous ether oxygens to solvate one Li^+. The conformational change upon Li^+ solvation is minimal,[51] and such single-segment ether solvation does not lead to the entropic penalty associated with cross-linking.[20] The phenomenon discussed above can be better understood via a chelating mechanism in which a polydentate ligand is more entropically favorable than a monodentate ligand and thus has a higher affinity for the binding ion. In that context, a POEM side chain can be considered to be a polydentate ligand for Li^+, whereas a cyclic carbonate side chain is monodentate. Zhang et al. provided a similar argument for a series of glyme-LiTFSI ionic liquid electrolyte systems.[52]

The favorability of Li^+ solvation by ether molecules is further supported by the underlying populations of the solvation motifs. Solvation motifs describe the immediate environment of Li^+ and include the count of each type of oxygen and the number of solvating segments. Note that the number of solvating segments is included as an important criterion for

https://doi.org/10.1021/acs.macromol.3c00804
Macromolecules 2023, 56, 8069−8079

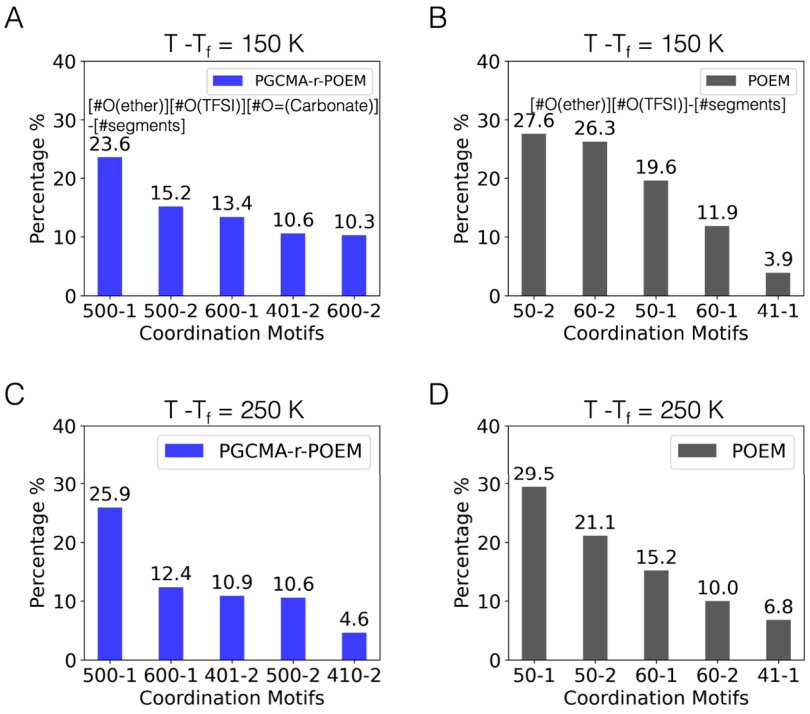

Figure 5. (A,B) Population of the five most abundant Li^+ coordination motifs in (A,C) PGCMA-*r*-POEM and (B,D) POEM. The simulations are at (A,B) $T - T_f = 150$ K and (C,D) $T - T_f = 250$ K. The binding motif denotes the counts of different oxygens present in the first solvation shell of Li^+ and the number of coordinating segments. For PGCMA-*r*-POEM, the first three digits refer to the counts of O(ether), O(TFSI), and O═(carbonate), respectively. For POEM, the first two digits refer to the count of O(ether) and O(TFSI), respectively. The digit following the dash refers to the number of coordinating chains. For example, 401-2 in PGCMA-*r*-POEM indicates a first solvation shell consisting of four ether oxygens from one OEM side chain, zero oxygen from TFSI anions, and one oxygen from a cyclic carbonate side chain. The presence of each TFSI molecule is treated as one segment. The presence of each O═(carbonate) is treated as one segment.

two reasons. First, it indicates the extent of cross-linking effects, and its statistics provide insights into the role of entropic driving forces in Li^+ solvation. Second, it gives insights into the relative importance of the two major Li^+ transport mechanisms: interchain and intrachain hopping.[22,25] Previous studies have shown that in POEM, intraside chain hopping is fast but local, while long-range Li^+ transport relies on interside chain hopping.[14,53] Although Li^+ hopping is a dynamic process, the time-averaged statistics on single-chain solvation versus multichain solvation can still provide helpful information about the relative importance of the two hopping mechanisms. Figure 5 presents the population of the five most abundant Li^+ solvation motifs in the POEM and PGCMA-*r*-POEM at two temperatures. These results show that Li^+ is primarily solvated by 5−6 ether oxygens. In PGCMA-*r*-POEM, the O═(carbonate) exhibits a slightly higher affinity to Li^+ than does the O(TFSI). Two-chain solvation is more likely to occur at low temperatures and decreases at elevated temperatures. Similarly, at a fixed temperature, two-chain solvation is more favorable in the POEM homopolymer than in the PGCMA-*r*-POEM copolymer. This highlights the impact of entropy on Li^+-ether solvation, as both a temperature increase and dilution amplify the entropic contributions to the total free energy. Note that single-chain solvation is preferred over two-chain solvation as the latter forms temporary cross-links that restrict polymer conformation and lead to a higher entropic penalty. The temperature dependence of the entropic driving force explains why single-chain solvation is favored at elevated temperatures. This trend toward single-chain solvation as temperature increases is also observed in the PEO/LiI system.[51] In the context of the chelate effect, the entropic favorability of multidentate ligands allows their binding to metal ions to be more resistant to dilution. In such materials, single-chain solvation involves a single POEM side chain donating six O(ether) to a Li^+, whereas two-chain solvation involves two side chains, each donating three O(ether) to the Li^+[22]. The higher number of solvating sites provided by the single side chain yields a stronger chelate. This is why single-chain solvation is favored in the copolymer, where the addition of PGCMA segments dilutes the concentration of the solvating O(ether).

The arguments presented above are also supported by past reports. For example, in a linear PEO-polycarbonate system, Li^+ is reported to be solvated mainly by the carbonate group and not by the ether segments, which are linearly copolymerized with the carbonate groups and take up only 30 mol %.[54] This is because these ether segments are frequently interrupted by carbonate units such that Li^+-ether solvation does not benefit from any entropic favorability. A separate study reported that when PGCMA-*r*-POEM is swollen with 1:1 EC:DMC solvent, Li^+ tends to be mainly solvated by the small-molecule EC solvent and only partially by the ether segments from the polymer matrix.[55] These results suggest that the interaction between Li^+ and cyclic carbonate groups varies depending on whether it is a small molecule or part of the polymer and that solvation by the former involves a favorable entropic gain when solvating Li^+.

In contrast to liquid electrolytes, where the high polarity of the EC facilitates salt dissociation, the role of cyclic carbonate groups in SPEs is less explicit. They are rarely found in the Li^+ solvation shell in PGCMA-*r*-POEM, but their presence dilutes the Li^+-solvating ether segments, leading to a shift in solvation

https://doi.org/10.1021/acs.macromol.3c00804
Macromolecules 2023, 56, 8069−8079

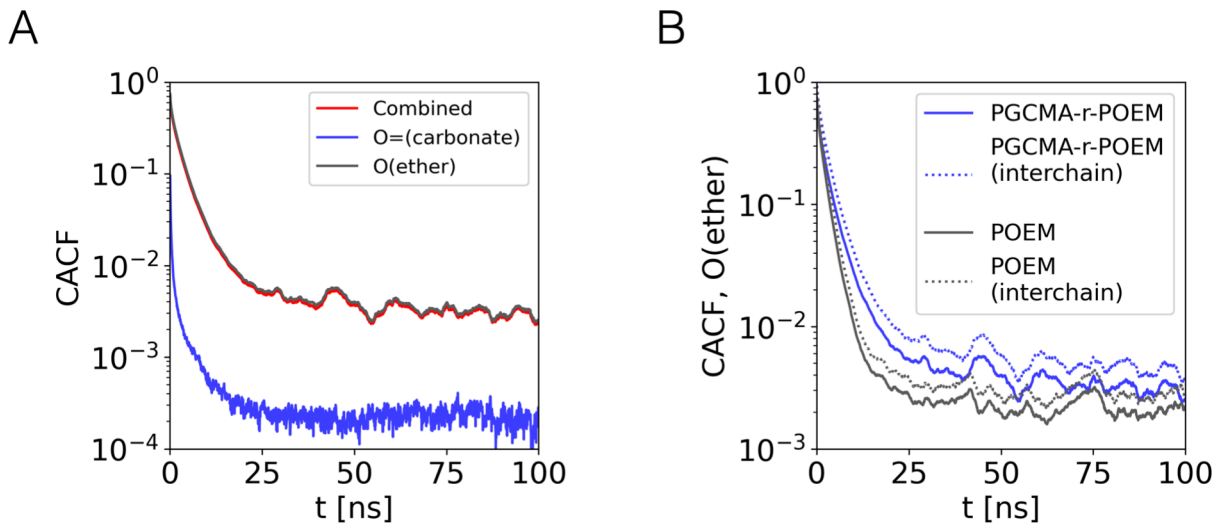

Figure 6. Coordination autocorrelation functions at a $T - T_f$ of 250 K. (A) Total CACF and its breakdown into the O(ether) contribution and the O═(carbonate) contribution in PGCMA-*r*-POEM. (B) Total CACF by O(ether) and their interchain O(ether) contribution in PGCMA-*r*-POEM and POEM. The total autocorrelation function considers both intraside chain and interside chain changes in the Li^+ first solvation shell members. The interchain autocorrelation functions consider replacements of Li^+ first solvation shell members by oxygens from different side chains.

preferences from two-chain solvation to single-chain solvation. This shift is expected to reduce the long-range transport of Li^+ by suppressing interchain hopping. When the shift is due to a temperature increase, its adverse effect on Li^+ transport is offset by a significant increase in the segmental dynamics. However, if the shift is caused by the dilution of ether segments at fixed segmental dynamics, a reduction in the rate of Li^+ hopping is expected, especially interchain hopping.

Presence of Carbonate Groups Has an Implicit Impact on Li^+ Hopping Mechanisms. To further characterize how the presence of O═(carbonate) in a coordination shell affects Li^+ transport, we calculated the coordination autocorrelation function (CACF), which quantifies how fast a Li^+ escapes from its current coordination environment.[22,23] It is defined as

$$\mathrm{CACF}(t) = \left\langle \frac{|S(t) \cap S(0)|}{|S(0)|} \right\rangle \tag{1}$$

where $S(0)$, $S(t)$ denote the sets of atoms present in the first solvation shell of a Li^+ at a starting time point and at a future time point t, respectively. $\cap$ is the intersection operator, $|\cdots|$ is the cardinality of the set, and $\langle\cdots\rangle$ denotes an ensemble average over time origins and Li^+ instances. The CACF defined here is an intermittent correlation function since the set of solvating oxygens is compared at the two ends of the time interval of interest. Figure 6A compares CACFs contributed by different oxygen types, which are determined as follows. The CACF for O═(carbonate) considers the decorrelation when the solvation shell at either time point contains O═(carbonate). The CACF of O(ether) considers the decorrelation when the solvation shells at both time points contain only O(ether). Our results show that the overall decorrelation in PGCMA-*r*-POEM is mostly due to the decorrelation from the O(ether) solvation shells, while the decorrelation from the O(carbonate) solvation shells is extremely fast and does not contribute much to the overall decorrelation. This is caused by the lower Li^+−O═(carbonate) coordination number compared to Li^+−O(ether), leading to frequent replacement of the Li^+-carbonate coordination, while the majority of the solvation shell, i.e., Li^+−O(ether) coordination, remains unchanged. The small contribution of the carbonate CACF to the total CACF supports the idea that the replacement of O═(carbonate) in a solvation shell does not lead to Li^+ displacement via hopping, but instead Li^+ movement relies on the slower replacement of O(ether), which is rate-limiting. The rate-limiting decorrelation of the Li^+−O(ether) solvation shell is due to both interchain and intrachain hopping. Figure 6B compares CACFs contributed by each mechanism in POEM and in PGCMA-*r*-POEM. The CACF of interchain hopping considers the decorrelation when the set of side chains involved in $S(t)$ is different from that involved in $S(0)$. In both systems, the first coordination shell members appear to be fully decorrelated after 30 ns. The total CACF decay is largely due to the decay of the interchain CACF, while the intrachain hopping contribution is small; a Li^+ that is typically solvated by five O(ether) along a side chain can only hop by a maximum of four O(ether) units on the same side chain. We find that the total decorrelation is faster in POEM than in PGCMA-*r*-POEM, and this difference in total CACF mainly results from the difference in interchain hopping rates.

To summarize, the analysis of the CACF indicates that Li^+ solvation by carbonate is transient and does not impact the overall CACF. Instead, the slower decay of the overall CACF in PGCMA-*r*-POEM is due to suppressed interchain hopping among O(ether) solvation sites.

Hybrid Solvation Sites Formed by PGCMA and Ether Segments at Their Microscopic Interface Facilitate the Percolation of the Solvation Site Network. The concept of solvation site connectivity, introduced in recent studies, describes the concentration and spatial arrangement of Li^+-solvating units in SPEs and provides a useful tool to connect the molecular structure of the SPE and its ability to transport Li^+.[19,21] Past reports have shown that differences in conductivity can be explained by differences in connectivity, provided that differences in segmental mobility are accounted for.[19,20,22] In what follows, we rely on solvation site connectivity to quantify the diluting effects of the added PGCMA on Li^+ transport. We begin our analysis by identifying viable solvation sites according to previously reported

https://doi.org/10.1021/acs.macromol.3c00804
Macromolecules 2023, 56, 8069−8079

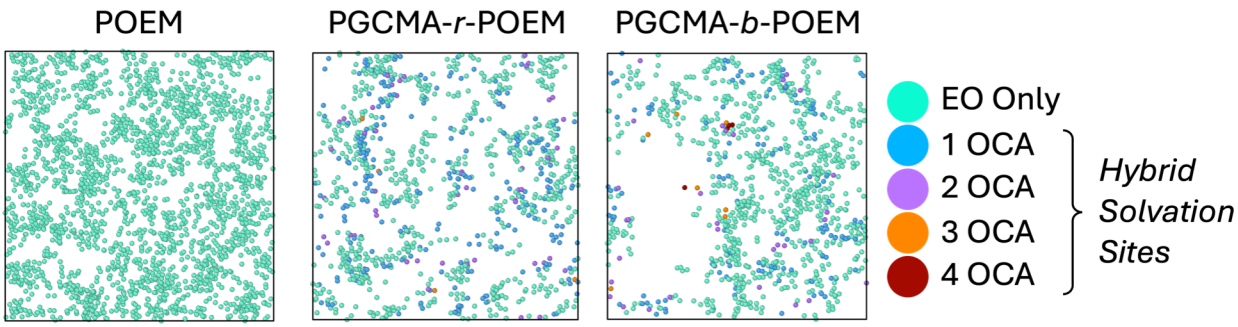

Figure 7. Visualization of viable solvation sites in (A) POEM, (B) PGCMA-*r*-POEM, and (C) PGCMA-*b*-POEM. The simulations are at $T - T_f = 150$ K. In (A), the viable solvation sites are colored by the O═(carbonate) composition: cyan sites are O(ether) only; blue, purple, orange, and red sites are hybrid sites containing one, two, three, and four O═(carbonate), respectively.

protocols.[19,20,22] Our calculations include all oxygen types in the polymer that participate in the first Li^+ solvation shell, including O═(carbonate). In Figure 7A,B, representative snapshots of identified solvation sites illustrate that the number density of solvation sites is lower in PGCMA-*r*-POEM than in POEM. Both systems, however, exhibit viable solvation sites that are distributed evenly throughout the simulation box. The corresponding connectivity κ is $(3.94 \pm 0.89) \times 10^{-4}$ in PGCMA-*r*-POEM, half of that of POEM $(7.85 \pm 1.15) \times 10^{-4}$. This ratio is consistent with the reported two-fold difference in conductivity observed in experiments.[29]

To further probe how Li^+ transport occurs in mixed SPEs, we extend our investigation to include the block copolymer PGCMA-*b*-POEM, which exhibits segmental dynamics near identical to those of the random copolymer but lower miscibility between POEM and PGCMA units. The idea of varying degrees of miscibility has been employed in a recent study to probe Li^+ transport in PEO/PMMA mixture electrolytes, because in those materials the PEO and PMMA segments coexist in a single phase macroscopically, while their local concentrations fluctuate depending on the degree of miscibility.[26] That study reported that an increased degree of miscibility worsens the conductivity by encouraging the solvation sites to group into isolated clusters on a critical length scale of 5−15 Å. In this study, the random and block copolymers exhibit pronounced differences in interchain packing at the same length scale, with the random copolymer being better mixed (Figure S7). In contrast to that study, for the PGCMA/POEM pair examined here, experiments find an opposite trend in conductivity: the more mixed random copolymer PGCMA-*r*-POEM exhibits higher conductivity than the block copolymer PGCMA-*b*-POEM.[29] Since local mixing leads to an inhomogeneous distribution of Li^+ solvation sites, characterizing Li^+ transport in mixed SPE requires an analysis that goes beyond solvation site connectivity.

The viable solvation sites can be further categorized based on their compositions of O(ether) and O═(carbonate), to highlight the relative contribution of each. Figure 7B indicates that in PGCMA-*r*-POEM, the PGCMA and POEM units mix to form hybrid viable solvation sites that include both O═(carbonate) and O(ether) over a wide range of compositions, as revealed by an abundance of blue, purple, and orange sites in the figure. This suggests that the solvation site network in PGCMA-*r*-POEM can percolate through a mixture of O(ether)-only and hybrid sites. In contrast, Figure 7C shows that in PGCMA-*b*-PMMA, the viable solvation sites are found to be either only ether (cyan sites) or contain many O═(carbonate) (orange and red sites), whereas hybrid sites that contain only one or two O═(carbonate) are less frequent. In contrast, Figure 7C shows that in PGCMA-*b*-PMMA, the majority of the identified viable solvation sites contain zero or only one O═(carbonate), whereas hybrid sites are rare. Visually, the distribution of these solvation sites also reflects a greater contrast of the local concentration in the block copolymers, where the ether-dominant sites tend to be in certain regions, while other areas are nearly void of solvation sites. Even in domains rich in PGCMA, few 4-carbonate solvation sites are found, possibly due to a higher steric hindrance associated with forming the all-carbonate solvation sites, despite the fact that sufficient O═(carbonate) are present. These isolated sites are possibly unreachable by Li^+ from other solvation sites. Because patches of PGCMA-rich domains in the block copolymer do not help with Li^+ solvation or transport, the overall solvation network is no longer connected. This is different from what is observed in liquid electrolytes, where Li^+ solvation by four carbonate units is common due to minimal steric hindrance. Finally, these results also reveal the critical role of interfacial sharpness in the formation and arrangement of viable solvation sites in the materials considered here. A diffuse interface between PGCMA-rich and POEM-rich domains allows O═(carbonate) to join the formation of hybrid solvation sites and leads to an overall denser and interconnected network, whereas a sharp interface effectively restricts the participation of the group of O═(carbonate) in Li^+ solvation.

The trends outlined above for the composition of viable solvation sites are consistent with the population distribution of Li^+ coordination motifs discussed earlier. The two concepts differ slightly, in that viable solvation sites are geometric centroids of groups of solvating oxygens that could host Li^+, whereas the coordination motifs correspond to the actual first solvation shells formed with Li^+. Figures S8 and 5A report the population of the five most abundant Li^+ coordination motifs in the block and random copolymers, respectively. A comparison between them shows that the population distribution of the top three motifs is nearly identical. However, the hybrid coordination motif 401-2, which involves four O(ether) from a POEM side chain and one O═(carbonate), is less frequent in the block copolymer than in the random copolymer. In the block copolymer, this hybrid motif is overtaken by the all-O(ether) motif 600-2. To further quantify the utilization of Li^+-solvating oxygens for solvation and transport, we compare the participation rates of O(ether) and O═(carbonate) in forming viable solvation sites. In

https://doi.org/10.1021/acs.macromol.3c00804
Macromolecules 2023, 56, 8069−8079

PGCMA-*r*-POEM, 85 ± 1% of the total O(ether) population and 41 ± 3% of the total O═(carbonate) population are expected to form viable solvation sites. In PGCMA-*b*-POEM, the participation rates are 83 ± 1 and 27 ± 3% for O(ether) and O═(carbonate), respectively. For reference, in POEM, the participation rate for O(ether) is 90 ± 1%. While the participation rate for O(ether) is consistently high across the three materials, there is a statistically significant reduction in O═(carbonate) participation in the block compared to the random copolymer. It is important to note that small-angle X-ray scattering data for the block copolymer indicates a characteristic length scale of 20 Å for local concentration fluctuations,[29] suggesting that simulations over larger length scales and time scales could provide better comparisons between the block and the random copolymer. Nonetheless, the results reported here provide a coherent physical picture of Li^+ solvation in the random versus the block copolymers and help explain their underlying conductivity differences.

CONCLUSIONS

Atomistic simulations have been used to investigate Li^+ solvation and transport in POEM homopolymers and their copolymers with PGCMA. The simulated ion mobilities are in agreement with experimental findings[29] and show that the reduction in Li^+ diffusivity in the copolymer persists even after accounting for segmental mobility T_g effects.

We find that entropic penalties govern the solvation tendency in copolymers of mixed polarity; Li^+−O(ether) solvation is preferred over that by the highly polar O═(carbonate). As the presence of PGCMA dilutes the concentration of O(ether), the solvation preference is shifted toward single-chain solvation, thereby decreasing interchain hopping. In addition to a change in the hopping mechanism, a disruption of the solvation site network also contributes to reduced Li^+ diffusivity. In particular, the solvation site connectivity decreases by 50% in the random copolymer compared to the homopolymer, consistent with the experimentally measured reduction in conductivity.[29] By further extending the analysis to random and block copolymers of PGCMA and POEM, we find that PGCMA units and ether segments can form hybrid solvation sites at diffuse nanoscopic interfaces. In the well-mixed random copolymer, these hybrid solvations create a percolating Li^+ transport network. In contrast, in the less-mixed block copolymer, regions that are enriched with PGCMA and depleted of POEM are transiently unavailable for Li^+ transport, as the formation of an all-carbonate solvation site is entropically unfavorable. Experimental conductivity differences between the random and block copolymers can therefore be explained through a difference in solvation site percolation due to different degrees of mixing.

ASSOCIATED CONTENT

Supporting Information

The Supporting Information is available free of charge on the ACS Publications Web site. The Supporting Information is available free of charge at https://pubs.acs.org/doi/10.1021/acs.macromol.3c00804.

Simulation methods, determination of fictive temperature, and calculation of dipole moments and dielectric constants (PDF)

AUTHOR INFORMATION

Corresponding Author

Juan J. de Pablo − *Pritzker School of Molecular Engineering, University of Chicago, Chicago, Illinois 60637, United States; Center for Molecular Engineering and Materials Science Division, Argonne National Laboratory, Lemont, Illinois 60439, United States;* orcid.org/0000-0002-3526-516X; Email: depablo@uchicago.edu

Authors

Chuting Deng − *Pritzker School of Molecular Engineering, University of Chicago, Chicago, Illinois 60637, United States;* orcid.org/0000-0002-0416-178X

Peter Bennington − *Pritzker School of Molecular Engineering, University of Chicago, Chicago, Illinois 60637, United States;* orcid.org/0000-0002-0501-1441

Regina J. Sánchez-Leija − *Pritzker School of Molecular Engineering, University of Chicago, Chicago, Illinois 60637, United States;* orcid.org/0000-0003-1506-6443

Shrayesh N. Patel − *Pritzker School of Molecular Engineering, University of Chicago, Chicago, Illinois 60637, United States; Center for Molecular Engineering, Argonne National Laboratory, Lemont, Illinois 60439, United States;* orcid.org/0000-0003-3657-827X

Paul F. Nealey − *Pritzker School of Molecular Engineering, University of Chicago, Chicago, Illinois 60637, United States; Center for Molecular Engineering and Materials Science Division, Argonne National Laboratory, Lemont, Illinois 60439, United States;* orcid.org/0000-0003-3889-142X

Complete contact information is available at: https://pubs.acs.org/10.1021/acs.macromol.3c00804

Author Contributions

The manuscript was written with contributions of all authors. The authors declare no competing financial interests.

Notes

The authors declare no competing financial interest.

ACKNOWLEDGMENTS

We gratefully acknowledge support by the U.S. Department of Energy (DOE), Basic Energy Sciences (BES), Materials Sciences and Engineering Division (MSE). The simulations were completed on computational resources provided by the University of Chicago Research Computing Center. Some of the calculations presented in this work were carried out using software developed with support from the DOE, BES, MSE, through the Midwest Integrated Center for Computational Materials (MICCoM).

REFERENCES

(1) Patel, S. N. 100th Anniversary of Macromolecular Science Viewpoint: Solid Polymer Electrolytes in Cathode Electrodes for Lithium Batteries. Current Challenges and Future Opportunities. *ACS Macro Lett.* **2021**, *10* (1), 141−153.

(2) Ketkar, P. M.; Shen, K. H.; Hall, L. M.; Epps, T. H. Charging toward Improved Lithium-Ion Polymer Electrolytes: Exploiting Synergistic Experimental and Computational Approaches to Facilitate Materials Design. *Mol. Syst. Des. Eng.* **2019**, *4* (2), 223−238.

(3) Xue, Z.; He, D.; Xie, X. Poly(Ethylene Oxide)-Based Electrolytes for Lithium-Ion Batteries. *J. Mater. Chem. A* **2015**, *3* (38), 19218−19253.

(4) Hallinan, D. T.; Balsara, N. P. Polymer Electrolytes. *Annu. Rev. Mater. Res.* **2013**, *43* (1), 503−525.

(5) Hanson, B.; Pryamitsyn, V.; Ganesan, V. Mechanisms Underlying Ionic Mobilities in Nanocomposite Polymer Electrolytes. *ACS Macro Lett.* **2013**, *2* (11), 1001−1005.
(6) Young, W. S.; Albert, J. N. L.; Schantz, A. B.; Epps, T. H. Mixed-Salt Effects on the Ionic Conductivity of Lithium-Doped PEO-Containing Block Copolymers. *Macromolecules* **2011**, *44* (20), 8116−8123.
(7) Young, W. S.; Kuan, W. F.; Epps, T. H. Block Copolymer Electrolytes for Rechargeable Lithium Batteries. *J. Polym. Sci., Part B: Polym. Phys.* **2014**, *52*, 1−16. January
(8) Gomez, E. D.; Panday, A.; Feng, E. H.; Chen, V.; Stone, G. M.; Minor, A. M.; Kisielowski, C.; Downing, K. H.; Borodin, O.; Smith, G. D.; Balsara, N. P. Effect of Ion Distribution on Conductivity of Block Copolymer Electrolytes. *Nano Lett.* **2009**, *9* (3), 1212−1216.
(9) Sethuraman, V.; Mogurampelly, S.; Ganesan, V. Multiscale Simulations of Lamellar PS−PEO Block Copolymers Doped with LiPF 6 Ions. *Macromolecules* **2017**, *50* (11), 4542−4554.
(10) Sethuraman, V.; Mogurampelly, S.; Ganesan, V. Ion Transport Mechanisms in Lamellar Phases of Salt-Doped PS−PEO Block Copolymer Electrolytes. *Soft Matter* **2017**, *13*, 7793−7803.
(11) Bouchet, R.; Maria, S.; Meziane, R.; Aboulaich, A.; Lienafa, L.; Bonnet, J. P.; Phan, T. N. T.; Bertin, D.; Gigmes, D.; Devaux, D.; Denoyel, R.; Armand, M. Single-Ion BAB Triblock Copolymers as Highly Efficient Electrolytes for Lithium-Metal Batteries. *Nat. Mater.* **2013**, *12* (5), 452−457.
(12) Xu, K. Nonaqueous Liquid Electrolytes for Lithium-Based Rechargeable Batteries. *Chem. Rev.* **2004**, *104* (10), 4303−4417.
(13) Wheatle, B. K.; Lynd, N. A.; Ganesan, V. Effect of Polymer Polarity on Ion Transport: A Competition between Ion Aggregation and Polymer Segmental Dynamics. *ACS Macro Lett.* **2018**, *7* (10), 1149−1154.
(14) Webb, M. A.; Jung, Y.; Pesko, D. M.; Savoie, B. M.; Yamamoto, U.; Coates, G. W.; Balsara, N. P.; Wang, Z. G.; Miller, T. F. Systematic Computational and Experimental Investigation of Lithium-Ion Transport Mechanisms in Polyester-Based Polymer Electrolytes. *ACS Cent. Sci.* **2015**, *1* (4), 198−205.
(15) Pesko, D. M.; Jung, Y.; Hasan, A. L.; Webb, M. A.; Coates, G. W.; Miller, T. F.; Balsara, N. P. Effect of Monomer Structure on Ionic Conductivity in a Systematic Set of Polyester Electrolytes. *Solid State Ion* **2016**, *289*, 118−124.
(16) Sharon, D.; Bennington, P.; Dolejsi, M.; Webb, M. A.; Dong, B. X.; de Pablo, J. J.; Nealey, P. F.; Patel, S. N. Intrinsic Ion Transport Properties of Block Copolymer Electrolytes. *ACS Nano* **2020**, *14*, 8902−8914.
(17) Sharon, D.; Bennington, P.; Webb, M. A.; Deng, C.; De Pablo, J. J.; Patel, S. N.; Nealey, P. F. Molecular Level Differences in Ionic Solvation and Transport Behavior in Ethylene Oxide-Based Homopolymer and Block Copolymer Electrolytes. *J. Am. Chem. Soc.* **2021**, *143* (8), 3180−3190.
(18) Kuan, W. F.; Remy, R.; Mackay, M. E.; Epps, T. H. Controlled Ionic Conductivity via Tapered Block Polymer Electrolytes. *RSC Adv.* **2015**, *5* (17), 12597−12604.
(19) Pesko, D. M.; Webb, M. A.; Jung, Y.; Zheng, Q.; Miller, T. F.; Coates, G. W.; Balsara, N. P. Universal Relationship between Conductivity and Solvation-Site Connectivity in Ether-Based Polymer Electrolytes. *Macromolecules* **2016**, *49* (14), 5244−5255.
(20) Bennington, P.; Deng, C.; Sharon, D.; Webb, M. A.; de Pablo, J. J.; Nealey, P. F.; Patel, S. N. Role of Solvation Site Segmental Dynamics on Ion Transport in Ethylene-Oxide Based Side-Chain Polymer Electrolytes. *J. Mater. Chem. A* **2021**, *9* (15), 9937−9951.
(21) Webb, M. A.; Savoie, B. M.; Wang, Z. G.; Miller, T. F. Chemically Specific Dynamic Bond Percolation Model for Ion Transport in Polymer Electrolytes. *Macromolecules* **2015**, *48* (19), 7346−7358.
(22) Deng, C.; Webb, M. A.; Bennington, P.; Sharon, D.; Nealey, P. F.; Patel, S. N.; de Pablo, J. J. Role of Molecular Architecture on Ion Transport in Ethylene Oxide-Based Polymer Electrolytes. *Macromolecules* **2021**, *54* (5), 2266−2276.
(23) Chu, W.; Webb, M.; Deng, C.; Colon, Y.; Kambe, Y.; Krishnan, S.; Nealey, P.; de Pablo, J. Understanding Ion Mobility in P2VP/NMP$^+$I$^-$ Polymer Electrolytes: A Combined Simulation and Experimental Study. *Macromolecules* **2020**, *53* (8), 2783−2792.
(24) Tobishima, S.; Morimoto, H.; Aoki, M.; Saito, Y.; Inose, T.; Fukumoto, T.; Kuryu, T. Glyme-Based Nonaqueous Electrolytes for Rechargeable Lithium Cells. *Electrochim. Acta* **2004**, *49* (6), 979−987.
(25) Borodin, O.; Smith, G. D. Mechanism of Ion Transport in Amorphous Poly(Ethylene Oxide)/LiTFSI from Molecular Dynamics Simulations. *Macromolecules* **2006**, *39* (4), 1620−1629.
(26) Sharon, D.; Deng, C.; Bennington, P.; Webb, M. A.; Patel, S. N.; de Pablo, J. J.; Nealey, P. F. Critical Percolation Threshold for Solvation-Site Connectivity in Polymer Electrolyte Mixtures. *Macromolecules* **2022**, *55* (16), 7212−7221.
(27) Sacristan, J.; Chen, C.; Maranas, J. K. Role of Effective Composition on Dynamics of PEO-PMMA Blends. *Macromolecules* **2008**, *41* (14), 5466−5476.
(28) Sethuraman, V.; Ganesan, V. Segmental Dynamics in Lamellar Phases of Tapered Copolymers. *Soft Matter* **2016**, *12*, 7818−7823.
(29) Bennington, P.; Sánchez-Leija, R. J.; Deng, C.; Sharon, D.; de Pablo, J. J.; Patel, S. N.; Nealey, P. F. Mixed-Polarity Copolymers Based on Ethylene Oxide and Cyclic Carbonate: Insights into Li-Ion Solvation and Conductivity. *Macromolecules* **2023**, *56* (11), 4244−4255.
(30) Martin, M. G.; Siepmann, J. I. Transferable Potentials for Phase Equilibria. 1. United-Atom Description of n-Alkanes. *J. Phys. Chem. B* **1998**, *102* (14), 2569−2577.
(31) Stubbs, J. M.; Potoff, J. J.; Siepmann, J. I. Transferable Potentials for Phase Equilibria. 6. United-Atom Description for Ethers, Glycols, Ketones, and Aldehydes. *J. Phys. Chem. B* **2004**, *108* (45), 17596−17605.
(32) Maerzke, K. A.; Schultz, N. E.; Ross, R. B.; Siepmann, J. I. TraPPE-UA Force Field for Acrylates and Monte Carlo Simulations for Their Mixtures with Alkanes and Alcohols. *J. Phys. Chem. B* **2009**, *113* (18), 6415−6425.
(33) Wick, C. D.; Theodorou, D. N. Connectivity-Altering Monte Carlo Simulations of the End Group Effects on Volumetric Properties for Poly(Ethylene Oxide). *Macromolecules* **2004**, *37* (18), 7026−7033.
(34) Wu, H.; Wick, C. D. Computational Investigation on the Role of Plasticizers on Ion Conductivity in Poly(Ethylene Oxide) LiTFSI Electrolytes. *Macromolecules* **2010**, *43* (7), 3502−3510.
(35) Canongia Lopes, J. N.; Pádua, A. A. H. Molecular Force Field for Ionic Liquids Composed of Triflate or Bistriflylimide Anions. *J. Phys. Chem. B* **2004**, *108* (43), 16893−16898.
(36) Kamath, G.; Robinson, J.; Potoff, J. J. Application of TraPPE-UA Force Field for Determination of Vapor−Liquid Equilibria of Carboxylate Esters. *Fluid Phase Equilib.* **2006**, *240* (1), 46−55.
(37) Wick, C. D.; Martin, M. G.; Siepmann, J. I. Transferable Potentials for Phase Equilibria. 4. United-Atom Description of Linear and Branched Alkenes and Alkylbenzenes. *J. Phys. Chem. B* **2000**, *104* (33), 8008−8016.
(38) Soetens, J.-C.; Millot, C.; Maigret, B.; Bakó, I. Molecular Dynamics Simulation and X—Ray Diffraction Studies of Ethylene Carbonate, Propylene Carbonate and Dimethyl Carbonate in Liquid Phase. *J. Mol. Liq.* **2001**, *92* (3), 201−216.
(39) Chaudhari, M. I.; Nair, J. R.; Pratt, L. R.; Soto, F. A.; Balbuena, P. B.; Rempe, S. B. Scaling Atomic Partial Charges of Carbonate Solvents for Lithium Ion Solvation and Diffusion. *J. Chem. Theory Comput.* **2016**, *12* (12), 5709−5718.
(40) Frisch, M. J.; Trucks, G. W.; Schlegel, H. B.; Scuseria, G. E.; Robb, M. A.; Cheeseman, J. R.; Scalmani, G.; Barone, V.; Petersson, G. A.; Nakatsuji, H.; Li, X.; Caricato, M.; Marenich, A.; Bloino, J.; Janesko, B. G.; Gomperts, R.; Mennucci, B.; Hratchian, H. P.; Ort, J. V.; Fox, D. J. *Gaussian 09, Revision A.02*; Gaussian, Inc.: Wallingford CT, 2016.
(41) Breneman, C. M.; Wiberg, K. B. Determining Atom-Centered Monopoles from Molecular Electrostatic Potentials. The Need for High Sampling Density in Formamide Conformational Analysis. *J. Comput. Chem.* **1990**, *11* (3), 361−373.

https://doi.org/10.1021/acs.macromol.3c00804
Macromolecules 2023, 56, 8069−8079

(42) Brooks, D. J.; Merinov, B. V.; Goddard, W. A.; Kozinsky, B.; Mailoa, J. Atomistic Description of Ionic Diffusion in PEO−LiTFSI: Effect of Temperature, Molecular Weight, and Ionic Concentration. *Macromolecules* **2018**, *51* (21), 8987−8995.
(43) Plimpton, S. Fast Parallel Algorithms for Short-Range Molecular Dynamics. *J. Comput. Phys.* **1995**, *117* (1), 1−19.
(44) Brown, W. M.; Kohlmeyer, A.; Plimpton, S. J.; Tharrington, A. N. Implementing Molecular Dynamics on Hybrid High Performance Computers − Particle−Particle Particle-Mesh. *Comput. Phys. Commun.* **2012**, *183* (3), 449−459.
(45) Wheatle, B. K.; Keith, J. R.; Mogurampelly, S.; Lynd, N. A.; Ganesan, V. Influence of Dielectric Constant on Ionic Transport in Polyether-Based Electrolytes. *ACS Macro Lett.* **2017**, *6* (12), 1362−1367.
(46) Dahbi, M.; Ghamouss, F.; Tran-Van, F.; Lemordant, D.; Anouti, M. Comparative Study of EC/DMC LiTFSI and LiPF6 Electrolytes for Electrochemical Storage. *J. Power Sources* **2011**, *196* (22), 9743−9750.
(47) Shen, K.-H.; Hall, L. M. Effects of Ion Size and Dielectric Constant on Ion Transport and Transference Number in Polymer Electrolytes. *Macromolecules* **2020**, *53* (22), 10086−10096.
(48) Wheatle, B. K.; Keith, J. R.; Mogurampelly, S.; Lynd, N. A.; Ganesan, V. Influence of Dielectric Constant on Ionic Transport in Polyether-Based Electrolytes. *ACS Macro Lett.* **2017**, *6* (12), 1362−1367.
(49) Flory, P. J. Themodynamics of High Polymer Solutions. *J. Chem. Phys.* **1942**, *10* (1), 51−61.
(50) Schantz, S. On the Ion Association at Low Salt Concentrations in Polymer Electrolytes; a Raman Study of NaCF3SO3 and LiClO4 Dissolved in Polypropylene Oxide. *J. Chem. Phys.* **1991**, *94* (9), 6296−6306.
(51) Borodin, O.; Smith, G. D. Molecular Dynamics Simulations of Poly(Ethylene Oxide)/LiI Melts. 1. Structural and Conformational Properties. *Macromolecules* **1998**, *31* (23), 8396−8406.
(52) Zhang, C.; Ueno, K.; Yamazaki, A.; Yoshida, K.; Moon, H.; Mandai, T.; Umebayashi, Y.; Dokko, K.; Watanabe, M. Chelate Effects in Glyme/Lithium Bis(Trifluoromethanesulfonyl)Amide Solvate Ionic Liquids. I. Stability of Solvate Cations and Correlation with Electrolyte Properties. *J. Phys. Chem. B* **2014**, *118* (19), 5144−5153.
(53) Willner, L.; Poppe, A.; Allgaier, J.; Monkenbusch, M.; Lindner, P.; Richter, D. Micellization of Amphiphilic Diblock Copolymers: Corona Shape and Mean-Field to Scaling Crossover. *Europhys. Lett.* **2000**, *51* (6), 628−634.
(54) Morioka, T.; Nakano, K.; Tominaga, Y. Ion-Conductive Properties of a Polymer Electrolyte Based on Ethylene Carbonate/Ethylene Oxide Random Copolymer. *Macromol. Rapid Commun.* **2017**, *38* (8), No. 1600652.
(55) Tillmann, S. D.; Isken, P.; Lex-Balducci, A. Lithium Coordination in Cyclic-Carbonate-Based Gel Polymer Electrolyte. *J. Phys. Chem. C* **2015**, *119* (27), 14873−14878.

https://doi.org/10.1021/acs.macromol.3c00804
Macromolecules 2023, 56, 8069−8079